CHEMICAL ENGINEERING TRANSACTIONS
VOL. 100, 2023
A publication of AIDIC
The Italian Association of Chemical Engineering
Online at www.cetjournal.it
Guest Editors: Sauro Pierucci, Flavio Manenti

ISBN 979-12-81206-03-8; **ISSN** 2283-9216
DOI: 10.3303/CET23100062

Boosting Hydrodynamic Chromatography through DC-Electroosmotic Flows

Valentina Biagioni

Dipartimento Di Ingegneria Chimica Materiali Ambiente, Sapienza Università di Roma,via Eudossiana, 00184 Roma, Italy
valentina.biagioni@uniroma1.it

Open Tubular Hydrodynamic Chromatography (OTHDC) is currently limited by two shortcomings, namely the low selectivity and the large values of the Height Equivalent of the Theoretical Plate (HETP) caused by the Taylor-Aris dispersion. Recently, these authors and co-workers, (Biagioni and Cerbelli, 2022) have shown the possibility to contain the Taylor-Aris effect by inducing transversal velocity components superimposed to the main pressure-driven axial flow in a square channel. It was found that the separation efficiency can be enhanced by a 50-fold factor introducing a transversal DC-electroosmotic flow characterized by two symmetrical vortices. Considering the significant improvement obtained, the possibility to increase the efficiency of OTHDC by inducing different transversal flows is here investigated. Different transversal flows can be generated by placing electrode pairs in different configurations along the walls of the channel and by treating the walls with different coatings that make them charged or uncharged. It is found that all the types of transversal flows studied can improve the separation efficiency of OTHDC. The best performance is provided by the transversal flow characterized by four symmetrical vortices, which yield an improvement of the separation efficiency by a factor of up to one hundred times compared to standard OTHDC in the range of operating conditions considered.

1. Introduction

Open Tubular Hydrodynamic Chromatography (OTHDC) is a microfluidic size-based separation technique. It can be used to separate particles ranging from tens of nanometers to few micrometers. Examples of separation targets are DNA fragments (Wang et al., 2021) or polymer mixtures (Tijssen et al., 1983). OTHDC columns consist of an open channel with a characteristic cross-sectional dimension between 1-30 μm. Due to the micrometric size of the channel cross-section, the Reynolds number (Re) of the eluent (which is forced through the channel by an overall pressure drop) is below unity. Therefore, the momentum transport equations satisfy the Stokes flow regime. The separation mechanism of OTHDC is based on the interaction between the non-uniform axial flow, transverse diffusion, and hindrance effects due to the finite size of particles that must be separated. Due to transverse diffusion, particles move across all the possible flow streamlines, thus averaging out the axial velocity profile of the eluent as they flow downstream the channel. At the same time, particles are prevented from experiencing the low velocity streamlines close to the channel walls due to the hindrance associated with their finite size. The larger the particles, the larger the excluded low-velocity region. As a result, the driving force of OTHDC is based on the increasing function of average particle velocity with respect to particle size (Brewer, 2021). Figure 1 depicts the separation mechanism of OTHDC.

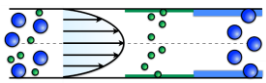

Figure 1: Separation mechanism of pressure driven OTHDC.

OTHDC separation mechanism is based on the difference between the average particle velocities (henceforth selectivity). The dependence of the average particle velocity on the particle size is typically weak. For this

Paper Received: 11 January 2023; Revised: 10 April 2023; Accepted: 8 June 2023
Please cite this article as: Biagioni V., 2023, Boosting Hydrodynamic Chromatography Through Dc-electroosmotic Flows, Chemical Engineering Transactions, 100, 367-372 DOI:10.3303/CET23100062

reason, the selectivity is low and OTHDC is characterized by low efficiency. Consequently, OTHDC requires lengthy channels to achieve a unitary resolution between two species. Further, the low efficiency is caused by the well-known Taylor-Aris effect, which increases the Height-Equivalent of the Theoretical Plate (henceforth $HETP_p$) as the eluent velocities increase. The $HETP_p$ can be defined as the squared dispersion bandwidth of particles of finite size recorded at a given time after the injection scaled to the distance traveled by the peak of the distribution in the same time interval. Therefore, $HETP_p$ is a measure of dispersion bandwidth of the species. In this regard, the separation resolution of OTHDC between two species "1" and "2" can be expressed as the ratio between the selectivity and the dispersion bandwidth of the two species. Various strategies to mitigate axial dispersion have been reported in the literature. The effect of the cross-section of the channel on the dispersion bandwidth of finite-size particles has been investigated by Biagioni et al., (2022). However, the most efficient way to contain the dispersion bandwidth has been reported by Zhao and Bau, (2007) and by Adrover (2013) in theoretical/numerical studies. They showed how the impact of axially invariant cross-sectional vortices generated by DC and AC-electroosmosis can contain the dispersion bandwidth of nonadsorbing solutes in a square channel. After nearly fifteen years, De Malsche and co-workers have experimentally demonstrated the positive effect of lateral vortices induced by AC-electroosmosis (Westerbeek et al., 2020) on axial dispersion for non-adsorbing/adsorbing solutes. In a recent article Biagioni and Cerbelli, (2022) predicted by a theoretical-numerical study the effects of cross-sectional flows characterized by two symmetrical vortices induced by DC-electroosmosis on the dispersion bandwidth of finite-sized particles. A 50-fold enhancement of the separation efficiency has been obtained in terms of reduction of the operating time compared to the standard case of OTHDC. In this work, the improvement of the separation efficiency of an OTHDC operation because of different secondary flows on the dispersion bandwidth of finite-size particles will be explained. This work is organized as follows: Section 2 describes the fluid dynamic problem, Section 3 explains the finite size particle transport model based on the Brenner Macro transport theory (Brenner et al., 1993), and finally, Section 4 shows the effect of different secondary flows on the separation efficiency of OTHDC for two different pairs of particle sizes.

2. System geometry and flow structures

A microchannel characterized by a square cross-section Ω and overall length L^* has been considered. The coordinates are made dimensionless with respect to the characteristic size of the cross-section, so that they can be considered in the interval $[0,1]X[0,1]X[0,L]$. A one-way coupling approximation is enforced throughout, where it is assumed that the suspended particles do not significantly perturb the flow structure, hence, the momentum transport can be considered as a single-phase problem. Due to the micrometric size of the channel cross-section, the Reynolds number is well below one, so the momentum transport is in the creeping flow regime. The velocity field is given by coupling an axial pressure-driven flow and an electrokinetically-induced transverse flow. Thus, an overall pressure drop is applied between the inlet and the outlet of the channel. Hence, the axial velocity component $w(x,y)$ can be determined solving a two-dimensional Poisson problem with no-slip boundary conditions enforced onto the walls of the cross-section:

$$\nabla_{\perp}^2 w = \frac{\partial P}{\partial z} \qquad w|_{x=0,1} = w|_{y=0,1} = 0 \qquad \text{Eq. 2.1}$$

where $\nabla_{\perp}^2 = \frac{\partial^2}{\partial x^2} + \frac{\partial^2}{\partial y^2}$ is the cross-sectional Laplacian operator.

The transverse flow $\boldsymbol{v}_{\perp}\big(u(x,y), v(x,y)\big)$ follows the two-dimensional Stokes equation

$$\nabla_{\perp}^2 v = \nabla_{\perp} P \qquad \text{Eq. 2.2}$$

coupled with slip/no-slip boundary conditions depending on the position of the electrode pair and the charges of the walls. Considering a pair of electrodes placed along opposite horizontal walls, if the right wall is positively charged, the boundary conditions become:

$$u|_{x=0,1} = u|_{y=0,1} = 0 \quad v|_{x=0} = v \quad v|_{x=1} = 0 \; and \; v|_{y=0,1} = 0$$

If two electrodes-free walls are oppositely charged, the boundary conditions become

$$u|_{x=0,1} = u|_{y=0,1} = 0 \quad v|_{x=0} = v, v|_{x=1} = -v \; and \; v|_{y=0,1} = 0$$

Finally, if half of the right and left walls are positively charged and the other half is negatively charged the boundary conditions are given by:

$$u|_{x=0,1} = 0, \quad u|_{y=0,1} = 0, v|_{x=0,1,y\epsilon[0-0.5]} = v \; v|_{x=0,1,y\epsilon[0.5-1]} = -v$$

Where v is the ratio between V_S (the Smoluchowsky velocity consistent with the thin double layer approximation (Lyklema, 2005) and the axial average velocity (U). The ratio v has been set equal to one. The boundary value problems characterized by Eq.2.1 and Eq. 2.2 and the corresponding boundary conditions have been solved using a finite element solver (COMSOL Multiphysics 5.5).

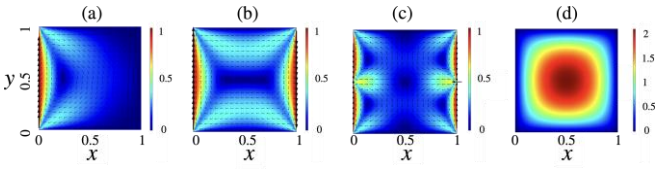

Figure 2: Panels (a), (b) and (c) depict the cross-sectional velocity profiles ($\boldsymbol{v}_{\perp}$) and cross-sectional arrows $\boldsymbol{w}(\boldsymbol{x},\boldsymbol{y})$. Panel (d) shows the axial velocity profile.

Panels (a), (b), (c) of Figure 2 depict the three different transverse flows: (a) cavity-flow, (b) 1-vortex flow, (c) 4-vortex flow. Panel (d) depicts the axial flow.

3. Transport model

This section briefly explains the theoretical transport model based on the Brenner Macro transport theory to estimate the separation performance of a chromatographic experiment, here expressed as the minimum length or the minimum operation time required to achieve a complete separation of a two-particle mixture. Particle dynamics can be evaluated by enforcing the one-way-coupling and the overdamped regime approximation (Maxey and Riley, 1983). The finite size of the particles can be taken into account by the excluded volume model. The excluded-volume model is based on the introduction of a particle transport domain (Ω_{r_p}) obtained by excluding a part of the volume normal to the solid walls of thickness equal to the particle radius. Brenner macro transport theory yields the axial transport properties (averaged over the channel cross-section) of the long-term dynamics of a particle distribution which is characterized by a Particle Number Density (PND), $c(x,y,z,t)$, where $c(x,y,z,t)dV$ is the fraction of particles into an elementary volume dV about (x,y,z) at time t. Initially, $t=0$, the PND is described by a uniform distribution $c_0(x,y,z,t=0)$, then the PND is governed by a micro transport advection-diffusion equation

$$\frac{\partial c}{\partial t} + v \cdot \nabla c = \frac{1}{Pe_p}\nabla^2 c \qquad \text{Eq.3.1}$$

equipped with no-flux boundary conditions on the boundary of the effective transport domain $\Omega_{\mathrm{r_p}}$.In Eq.3.1, $\boldsymbol{v}$ and Pe_p are the velocity field of the eluent and the particle Peclet number. The velocity field, $\boldsymbol{v}$, can be determined as discussed in the previous section. The particle Peclet number, Pe_p, is definite as $\mathrm{Pe}_p = \mathrm{U\,H}/\mathcal{D}_p$ where U is the average axial velocity, H is the characteristic size of the cross-channel section, and $\mathcal{D}_p$ the particle diffusivity. The latter can be quantified by the Stokes-Einstein equation as $\mathcal{D}_p = k_B\,T/(6\pi\mu r_p)$, where $k_B, T,$ and μ are the Boltzmann constant, the absolute temperature, and the dynamic viscosity, respectively. The micro transport advection-diffusion equation must be solved into the entire three-dimensional domain. In the case of OTHDC, the device is long thousands of times the characteristic size of the cross-channel section. This makes the approach to numerical solution of Eq. (3.3) unfeasible due to the large number of degrees of freedom necessary to obtain an accurate numerical solution. In this regard, the fundamental results of the Brenner macro transport theory is that the PND approaches, on the long-time scales, to a marginal distribution $C(z,t) = \int_{\Omega_{r_p}} c(x,y,z,t)\ dxdy / \int_{\Omega_{r_p}} dx\,dy$ that follows an *effective transport equation*

$$\frac{\partial C}{\partial t} + W_p^{\mathrm{eff}}\frac{\partial C}{\partial z} = \frac{1}{\mathrm{Pe}_p^{\mathrm{eff}}}\frac{\partial^2 C}{\partial^2 z} \qquad \text{Eq.3.2}$$

Where W_p^{eff} and $1/\mathrm{Pe}_p^{\mathrm{eff}}$ are the dimensionless effective velocity and dispersion coefficient related to a particle of a given size. The effective parameters can be estimated by solving two cascade boundary value problems (BVP), which are explained below. In the first one, a steady-state concentration $C_\infty(x,y) = \int_0^\infty \mathrm{c(x,y,z,t)\ dz}$ (the cross-section distribution projected onto a generic transversal section) must be introduced. From Eq.3.1 $C_\infty(x,y)$ is the solution of

$$\nabla_\perp \cdot J_\infty = 0; \quad J_\infty = v_\perp\, C_\infty - \frac{1}{\mathrm{Pe_p}}\nabla_\perp C_\infty \quad with \quad \mathbf{J}_\infty \cdot \mathbf{n} = 0 \ \ |_{\partial\Omega_{r_p}} \qquad \text{Eq.3.3}$$

The second BVP requires the introduction of a new function, the b-field $b(x,y)$, namely, the solution of the following advection-diffusion equation coupled with no-flux boundaries condition on the walls of the effective domain

$$\left(\nabla\perp\cdot\frac{1}{Pe_p}C_\infty\nabla_\perp b\right) - J_\infty\cdot\nabla_\perp b = C_\infty\left(W_p^{eff} - w\right) \qquad \text{with } \left(J_\infty b - \frac{1}{Pe_p}C_\infty\nabla_\perp b\right)\cdot n = 0 \qquad \text{Eq.3.4}$$

Once $C_\infty(x,y)$ and $b(x,y)$ have been determined the effective transport parameters can be estimated as:

$$W_p^{\text{eff}} = \int_{\Omega_{r_p}} w\ C_\infty\ dx\ dy \qquad \text{HETP}_p = \frac{1}{\text{Pe}_p^{\text{eff}}} = \frac{1}{\text{Pe}_p} + \int_{\Omega_{r_p}} C_\infty(\nabla_\perp b \cdot \nabla_\perp b)\ dx\ dy \qquad \text{Eq.3.5}$$

The two BVP problems can be solved numerically by using a finite solver COMSOL Multiphysics 5.5. Once the effective parameters have been estimated the minimum length, L, necessary to achieve a unitary resolution, namely, a complete separation of the two-particle mixture can be computed from:

$$R = \frac{1}{2}\frac{\left|\frac{1}{w_1^{\text{eff}}} - \frac{1}{w_2^{\text{eff}}}\right|\sqrt{L}}{\sqrt{\frac{2}{HETP_1\left(w_1^{\text{eff}}\right)^3}} + \sqrt{\frac{2}{HETP_2\left(w_2^{\text{eff}}\right)^3}}} = 1 \qquad \text{Eq.3.6}$$

Thus, Brenner's macro transport theory provides a theoretical framework for analysing a chromatographic experiment and for designing a microdevice where a given resolution value between two particle sizes can be achieved. In the next section, the effects of the interplay between the pure axial flow and the transversal flows (see Fig.2) on the effective parameters and the separation performance to varying the operating conditions for three particle sizes: $r_{p_1} = d_{p_1}/(2H) = 1/20$, $r_{p_2} = d_{p_2}/(2H) = 1/40$, and $r_{p_3} = d_{p_3}/(2H) = 1/80$ will be showed.

4. Results

4.1 C∞-Distribution and Effective Particle Velocity

The interaction between the transversal flows, particle diffusion, and particle size leads to localization effects in the solution of Eq. 3.3, $\boldsymbol{C}_\infty$. The localization effect is due to the no-flux boundary condition ($\mathbf{J}_\infty \cdot \mathbf{n} = 0\,|_{\partial\Omega_{r_p}}$) imposed on the boundary effective walls of the effective domain, Ω_{r_p},which depends on the particle radius and does not match with the fluid-dynamic domain Ω. For this reason, the normal components of the transversal velocity field on the effective walls are not null, so a counter-diffusive concentration gradient must occur to counterbalance the convective particle flow to assure the no-flux boundary conditions. The larger the particle radius, the larger the finite distance from the walls, the larger the normal components of the transversal velocity field on the effective boundary and the stronger non-uniformity of $\boldsymbol{C}_\infty$. When the effective domain coincides with the effective fluid dynamic domain (particle radius is zero) the $\boldsymbol{C}_\infty$ is strictly uniform. On the other hand, when Pe tends to zero, the cross-sectional distribution $\boldsymbol{C}_\infty$ shows an uniform distribution, in fact, Eq.3.3 becomes a pure diffusion equation, and the effect of the convective particle flow vanish. On the contrary, when Pe increases, $\boldsymbol{C}_\infty$ departs from the uniform distribution and the localization effects are strengthened. As can be gathered from Fig.3, if the particle Peclet number is increased the particles remain more and more entrapped inside the vortexes. Figure 3 depicts the $\boldsymbol{C}_\infty$ field correspondent to *Pe$_p$= 100 and 2000* for a particle size equal to $r_{p_1} = 1/20$ in the case of the three transversal flows considered in Sec.2.

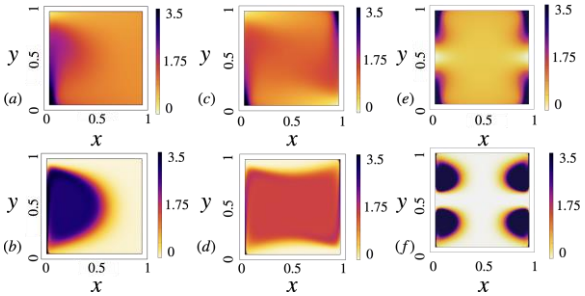

Figure 3: $\boldsymbol{C}_\infty$ estimated by solving Eq.3.3 referred to $r_p = 0.05$, at Pe$_p$= 100 and 2000. Panels (a-b) are referred to the cavity-flow, panels (c-d) to the 1-vortex flow and panels (e-f) to the 4-vortex flow.

The consequence of the nonuniform structure of the $\boldsymbol{C}_\infty$ is the non-monotonic behavior of W_p^{eff} depending on the Peclet number as shown in Fig.4. There W_p^{eff} is computed by weighting the axial average velocity with respect to $\boldsymbol{C}_\infty$. As consequence, the selectivity becomes a function dependent on Pe_p. When Pe_p is in the range between $[1-10]$, the selectivity is constant regardless of the structure of the cross-section flow. In this case, the localization effects of $\boldsymbol{C}_\infty$ become immaterial. If Pe_p is in the range $[10-100]$ the selectivity for both particle sizes decreases with respect to the selectivity of the OTHDC. At large values of Pe_p, the selectivity of cavity-flow case increases and overtakes the selectivity of the OTHDC for both particle sizes. On the contrary, in the 1-vortex flow case, the selectivity for both couples of particle size increases but only the selectivity referred to

the couple $r_{p1} = 0.025$ and $r_{p2} = 0.0125$ is enhanced with respect to the selectivity of OTHDC. In the case of 4-vortex transversal flow, the particle velocities decrease until they reach an intersection point at $Pe_p^* = 80$. When this occurs, the effective velocities are equal for all the particle sizes, the selectivity goes to zero and separation cannot occur. If Pe_p is larger than Pe_p^* , W_p^{eff} continues to decrease dependently on the particle size. The larger the particles, the stronger the localization effect of $\boldsymbol{C}_\infty$ on the lower velocity region, the smaller W_p^{eff}. An inversion of the dependence of effective velocity on particle size occurs. When Pe_p is larger than Pe_p^* the selectivity increases again, but it is always lower than that of standard OTHDC.

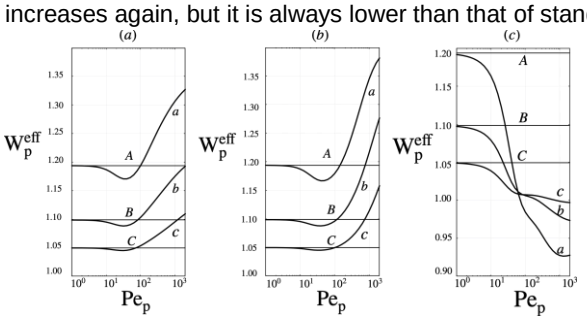

Figure 4: Effective velocity vs Pe$_p$ for $r_p = 0.05$ (curve a), $r_p = 0.025$ (curve b) and $r_p = 0.0125$(curve c). The lines A, B, and C depict the Pe$_p$-independent) effective velocity in standard OTHDC for the same particle sizes. Panels a,b,c are referred to the cavity-flow, 1-vortex flow and the 4-vortexes flow, respectively.

Thus, the interplay between the purely axial flow and the transversal-flows can cause a decrease of the selectivity and hence a reduction of the separation efficiency with respect to the OTHDC. In the next section, the consequences of the non-uniformity of $\boldsymbol{C}_\infty$ on axial dispersion will be evaluated.

4.2 Effective axial dispersion

The scaled $HETP_p$ can be determined by Eq. 3.6. Panels (a-c) of Fig.5 depict the comparison between $HETP_p$ for the purely axial flow (curves A-C) and in the presence of transversal flows (curves a-c). Panel (a), (b), and (c) refer to the cavity flow, the 1-vortex flow, and the 4-vortex flow, respectively. Curves A-a, B-b and C-c are referred to $r_{p3} = 0.0125$**,** $r_{p2} = 0.025$ and $r_{p1} = 0.05$, respectively. One can note how the maximum decrease of the $HETP_p$ is always associated with the bigger particle size. In fact, the bigger the particle, the stronger the localization effect of $\boldsymbol{C}_\infty$. One notes that $HETP_p$ referred to the biggest particle decreases by almost two decades in the case of the cavity flow and by three decades in the case of four vortexes. However, at large Pe_p values, the $HETP_p$ decreases in all the cases considered and it always enhances the separation performances of OTHDC, as shown in the next section.

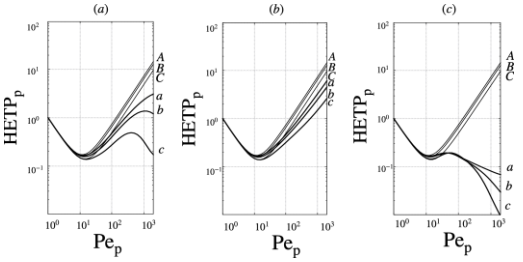

Figure 5: $HETP_p$ vs Pep for $r_p = 0.05$ (curve a), $r_p = 0.025$ (curve b) and $r_p = 0.0125$ (curve c).The curves A, B, and C depict the $HETP_p$ referred to the OTHDC for the same particle sizes. Panels a,b and c are referred to the cavity-flow, 1-vortex flow and the 4-vortex flow, respectively.

4.3 Separation efficiency

Next, the interplay between the W_p^{eff} and the $HETP_p$ on the minimum length (L) required to achieve a unitary resolution between a couple of particle sizes will be evaluated. In this section, Peclet number (Pe) is referred to the biggest particle size to assure the same operating conditions, (i.e., the same average axial velocity), hence $\text{Pe}=\text{Pe}_{r_{p1}}/\text{Pe}_{r_{p2}} = r_{p1}/r_{p2}$. Figure 6 shows the comparison between the minimum length vs Pe in the case of OTHDC (curves A, B) and in the presence of transversal flows. Curves A-a and B-b are referred to a mixture of particles characterized by $r_{p1} = 0.05$ and $r_{p2} = 0.025$ and $r_{p1} = 0.025$ and $r_{p2} = 0.0125$, respectively. As one

can note, when Pe is low, the minimum lengths required in the presence of transversal flows and in the case of purely axial flow coincide, i.e., the transversal flows have no impact on the device performance. When Pe is in the middle range of values the decrease of the selectivity causes a minimum length required in the presence of transversal flows larger than in the standard case. In these cases, the usage of the transversal flows is unfavourable. Finally, at large Pe values the presence of transversal flows enhances the separation performances of standard OTHDC. The minimum length required to assure the same resolution between $r_{p1} = 0.05$ and $r_{p2} = 0.025$ is provided by the presence of the 4-vortex flows and it is up to 100-fold times shorter than the minimum length required to purely axial OTHDC. Instead, the minimum length to obtain a unitary resolution between $r_{p1} = 0.025$ and $r_{p2} = 0.0125$ is provided by the cross-sectional cavity flow and it is more than twenty times shorter than standard OTHDC.

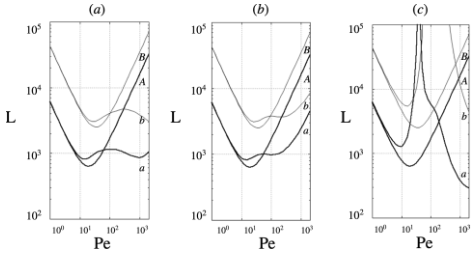

Figure 6: Minimum channel length yielding a unitary resolution vs Pe. Curves A, and a are referred to the cases for $r_p = 0.05$ and $r_p = 0.025$, respectively. Curves B, and b are referred to the cases for $r_p = 0.025$ and $r_p = 0.0125$ Curves labelled with capital letters refer to the OTHDC. Curves a, and b are referred to the case characterized by the cavity-flow (Panel (a)), 1-vortex flow (Panel (b)) and the 4-vortex flow (Panel (c)).

5. Conclusions

In this article, the improvement due to different streamlines of cross-sectional flows generated by DC-electroosmosis onto the separation performances of OTHDC has been shown. Different operating conditions and different cross-sectional flows have been analysed to find the best design and yield the maximum efficiency. The best performances are provided by the cross-sectional cavity flow related to the couple of particles sizes ($r_{p1} = 0.025\ and\ r_{p2} = 0.0125$) and by the 4-vortex flow referred to the couple of particle sizes ($r_{p1} = 0.05\ and\ r_{p2} = 0.025$). In these cases, the length of the device can be decreased up to 20 times and 100 times over the standard HDC, respectively. In this regard, future work will be focused on improving the separation efficiency by shaping the cross-sectional geometry, namely, the streamlines of the cross-sectional DC-electroosmotic flows or by investigating the effect of cross-sectional flows generated by AC-electroosmosis.

References

Adrover, A. (2013). Effect of secondary flows on dispersion in finite-length channels at high Peclet numbers. Physics of Fluids, 25(9), 093601.

Biagioni, V., & Cerbelli, S. (2022 a). 50-Fold Reduction of Separation Time in Open-Channel Hydrodynamic Chromatography via Lateral Vortices. Analytical Chemistry, 94(27), 9872-9879.

Biagioni, V., Cerbelli, S., & Desmet, G. (2022 b). Shape-Enhanced Open-Channel Hydrodynamic Chromatography. Analytical Chemistry, 94(46), 15980-15986.

Brenner, H., & Edwards, D. A. (1993). Macrotransport processes. Butterworth-Heinemann.

Brewer, A. K. (2021). Hydrodynamic chromatography: the underutilized size-based separation technique. Chromatographia, 84(9), 807-811.

Lyklema, J. (2005). Fundamentals of interface and colloid science: soft colloids (Vol. 5). Elsevier.

Maxey, M. R., & Riley, J. J. (1983). Equation of motion for a small rigid sphere in a nonuniform flow. The Physics of Fluids, 26(4), 883-889.

Tijssen, R., Bleumer, J. P. A., & Van Kreveld, M. E. (1983). Separation by flow (hydrodynamic chromatography) of macromolecules performed in open microcapillary tubes. Journal of Chromatography A, 260, 297-304.

Wang, Y., Zhou, Y., Zhang, D., Wang, X., & Liu, S. (2021). Extension of hydrodynamic chromatography to DNA fragment sizing and quantitation. Heliyon, 7(9), e07904.

Westerbeek, E. Y., Bomer, J. G., Olthuis, W., Eijkel, J. C., & De Malsche, W. (2020). Reduction of Taylor–Aris dispersion by lateral mixing for chromatographic applications. Lab on a Chip, 20(21), 3938-3947.

Zhao,H., & Bau, H. H. (2007). Effect of Secondary Flows on Taylor− Aris Dispersion. Analytical chemistry, 79(20), 7792-7798.